Mine Water and the Environment (2018) 37:393–404
https://doi.org/10.1007/s10230-017-0506-9

TECHNICAL ARTICLE

Relevance Between Hydrochemical and Hydrodynamic Data in a Deep Karstified Limestone Aquifer: a Mining Area Case Study

Wei Qiao[1] · Wenping Li[1] · Tao Li[2,3] · Xin Zhang[4] · Yangzhou Wang[4] · Youkuo Chen[4]

Received: 3 May 2017 / Accepted: 2 November 2017 / Published online: 16 December 2017

Abstract

Safe coal mining in a karst region requires that mining operations assess any disturbances in the hydrogeological functioning of local aquifers and flow systems, and determine if disruptions are likely in the mine. We studied the geologic, hydraulic, and geochemical characteristics of the deep Ordovician karstified aquifer in the Xinglongzhuang and Dongtan mines of the Yanzhou coal mining district (China). The presence of a 100 m deep research borehole in the Ordovician limestone aquifer nearby facilitated hydrochemical and hydrodynamic data collection. The buried depth affected karst rock porosity, and the reduced porosity increased karst development. This, in turn, affected the abundance of water in the karst fissure. In addition to calcite and dolomite, the Ordovician limestone contains gypsum, which dissolves to form sulfate ions. Hydraulic data revealed that the water abundance in the research area is comparatively low, except for the C8 syncline zone. The Ordovician strata in this area is located in the deep, slow-flow zone of a vertical karst aquifer system, and the drilling unit water inflow is very low, which could represent the water abundance of the aquifer. Understanding this complex flow system is critical to appropriately assess the area's deep groundwater resources and guide decision making regarding coal extraction.

Keywords Deep karst · Water chemistry · Water abundance · Principal component analysis · Hydrogeological parameter

Introduction

Carbonate karst terraces cover almost 20% of the earth's land surface, and the waters associated with karst aquifers supply almost a quarter of the world's population with water. China has widely distributed carbonate rocks, covering ≈3.25 million km^2. This includes bare karst, covering ≈1.25 million km^2, and covered or buried karst, spanning ≈2 million km^2 (Li 2010; Yu 1994).

✉ Wei Qiao
qiaowei@cumt.edu.cn

1 School of Resources and Geosciences, China University of Mining and Technology, Xuzhou 221116, Jiangsu, People's Republic of China

2 Post-Doctoral Mobile Research Centre of Geological Resources and Geological Engineering, Xi'an University of Science and Technology, Xi'an 710065, Shaanxi, People's Republic of China

3 Shaanxi Coal and Chemical Industry Group Ltd, Xi'an 710065, Shaanxi, People's Republic of China

4 Donghua Construction Company Limited, Yankuang Group, Zoucheng 273500, Shandong, People's Republic of China

Coal mining is occurring at greater depths in China, increasing the number of disasters caused by water inflow. The problem is complicated by the indeterminate nature of the deep karst hydrogeology and high water pressures. Increased risks have been created by confined aquifers below the coal seams; these risks directly impact mine safety and coal production (Wu et al. 2004, 2013; Wu and Wang 2006; Yu et al. 2007).

Obtaining hydraulic and hydrochemical information about deep karst aquifers is difficult (Daher et al. 2011). Hydraulic tests, ionic analysis, corrosion calculations, and hydrochemical data collected from deep exploratory boreholes are very important in analyzing the hydraulic and hydrochemical characteristics of deep karst aquifers. Other investigations have focused on defining the processes and chemical reactions that characterize groundwater mineralization (Fidelibus and Tulipano 1986; Han et al. 2014; Reddy 2013; Srinivasamoorthy et al. 2014). In a previous study, we described the hydrodynamic and water chemical characteristics of the deep karst aquifer in the Dongtan coal mine (Qiao et al. 2014).

We have since studied the Xinglongzhuang and Dongtan coal mines in eastern China to reveal the hydrogeological

characteristics of deep karst. We applied principal component analysis (PCA) to better understand the groundwater's chemical composition. Our main goal was to characterize a deep carbonate system. This required a hydrogeological investigation across a large, deep karst aquifer, including pumping tests, dynamic observation, initial geo-stress measurements, hydrogeochemistry tests, and flow field exposure at man-made release points. Water chemistry analysis was facilitated by boreholes in the research area.

Study Area

The research was conducted in the Xinglongzhuang and Dongtan mines of the Yanzhou mining district, Shandong, north China. These are large mines affiliated with Yanzhou Coal Mining Co., Ltd. Figure 1a shows the study area. The Ordovician limestone is the main aquifer in the Yanzhou coal field groundwater system (Bian et al. 2017). The sixth section of the Middle Ordovician, which is approximately 50–100 m thick, is a major mining hazard. The karst aquifer system in this field is a syncline, with a dip direction facing east and gentle dip angles of less than 10°. The axis shows a NE–SW trend. The Ordovician karst aquifer system covers an area of 1373 km^2 with a bare karst area of 181 km^2, a covered karst area of 772 km^2, and a buried karst area of 420 km^2 under the main coal seams. The area receives an average annual precipitation of 714 mm and has a mean air temperature of 14.4 °C. The eastern boundary of the karst aquifer is the Yishan fault; the western, northern, and southern boundaries are Ordovician sub-outcrops. Topographically, the area is a very flat Quaternary alluvial plain, which gradually drops in elevation from NE to SW, and ranges from 40 to 47 m above sea level.

At this site, the thickness of the aquiclude between the main mine working seam and the deep Ordovician limestone ranges from 53.8 to 111.58 m; the average thickness is 81.41 m. The top of the buried Ordovician limestone is 600–1100 m below the ground surface, and the water pressure at the top of the Ordovician layer is 7.20–11.24 MPa. The ultra-high confined karst from the floor poses a significant threat to coal mining.

The Xinglongzhuang and Dongtan mines are located close to the core of the Yanzhou syncline, in the northern portion of a piedmont alluvial plain, with a ground elevation ranging from 40 to 63 m. The overall structure is consistent with a monocline structure (Fig. 1). The major coal-bearing strata is the Carboniferous–Permian strata and the basement is the Ordovician limestone (Li 2016a). The coal is covered by a purple-red Upper Jurassic sandstone and thick Quaternary strata.

The #16 and 17 coal seams being extracted in the two coal mines are both about 1 m thick. Based on the lithology, thickness, water features, and burial conditions, the main water aquifers, from the #16 coal to the bottom of the Ordovician limestone, can be divided into two categories (Fig. 2). The first is the Carboniferous limestone aquifer, composed of the fractured Taiyuan and Benxi limestones, and its associated distribution of karstic limestone sub-aquifers, labeled L10, L11, L12, L13, and L14. Below the Carboniferous limestone aquifer is an ≈30–80 m thick aquitard, followed by coal seams, and another aquitard. The second aquifer category is the 450–750 m thick Ordovician limestone aquifer. The sedimentary basement of the coal measure strata has a lower layer of thick gray limestone, with some brecciated limestone and yellow-green marl. The upper layer consists of gray or dark gray thick-bedded limestone and dolomitic limestone with a little thin-bedded limestone. The karst fissure pressure of the Ordovician limestone in greatest in the Yangzhou syncline core, where the interface water pressure can reach 8–12 MPa. The regional Ordovician karst is influenced by the presence of fractured, soluble rock; karst development originates in this thick, soluble rock layer.

The Ordovician water outside the boundary and inside the coal field are hydraulically connected, and the overlying quaternary system water–sand layer also indirectly supplies the coal field aquifer. To reveal the hydrogeological characteristics, hydrodynamics, and chemistry in the deep area, a total of 45 holes were drilled. This included 25 surface Ordovician holes and 20 underground Ordovician holes, drilled from an underground tunnel (Fig. 1). Holes were drilled 100 m deep into the Ordovician aquifer.

Methods

Principal Component Analysis

PCA can reduce data dimensionality and reveal the internal relationship among variables (Li et al. 2013a; Wu et al. 2014). PCA provides significant insight into data matrix structures, using eigen vectors from a correlation matrix of the variable (Davis 2002; Stetzenbach et al. 2001). PCA can be done using an eigenvalue decomposition of a data covariance (or correlation) matrix or singular value decomposition of a data matrix, usually after mean centering (and normalization or Z-score development) of the data matrix for each attribute (Abdi and Williams 2010).

PCA has also been used to control the factors involved in deep fracture-karst development (Zargham 2009). In this study, PCA was applied to determine the significance of ion composition in groundwater. The PCA considered 54 samples and 12 variables, including: elevation, pH, total hardness, free carbon dioxide (CO_2), soluble solids content, total dissolved solids (TDS), $K^+ + Na^+$, Ca^{2+}, Mg^{2+}, Cl^-, SO_4^{2-}, and HCO_3^-. Niu et al. (2011) list six steps to conduct

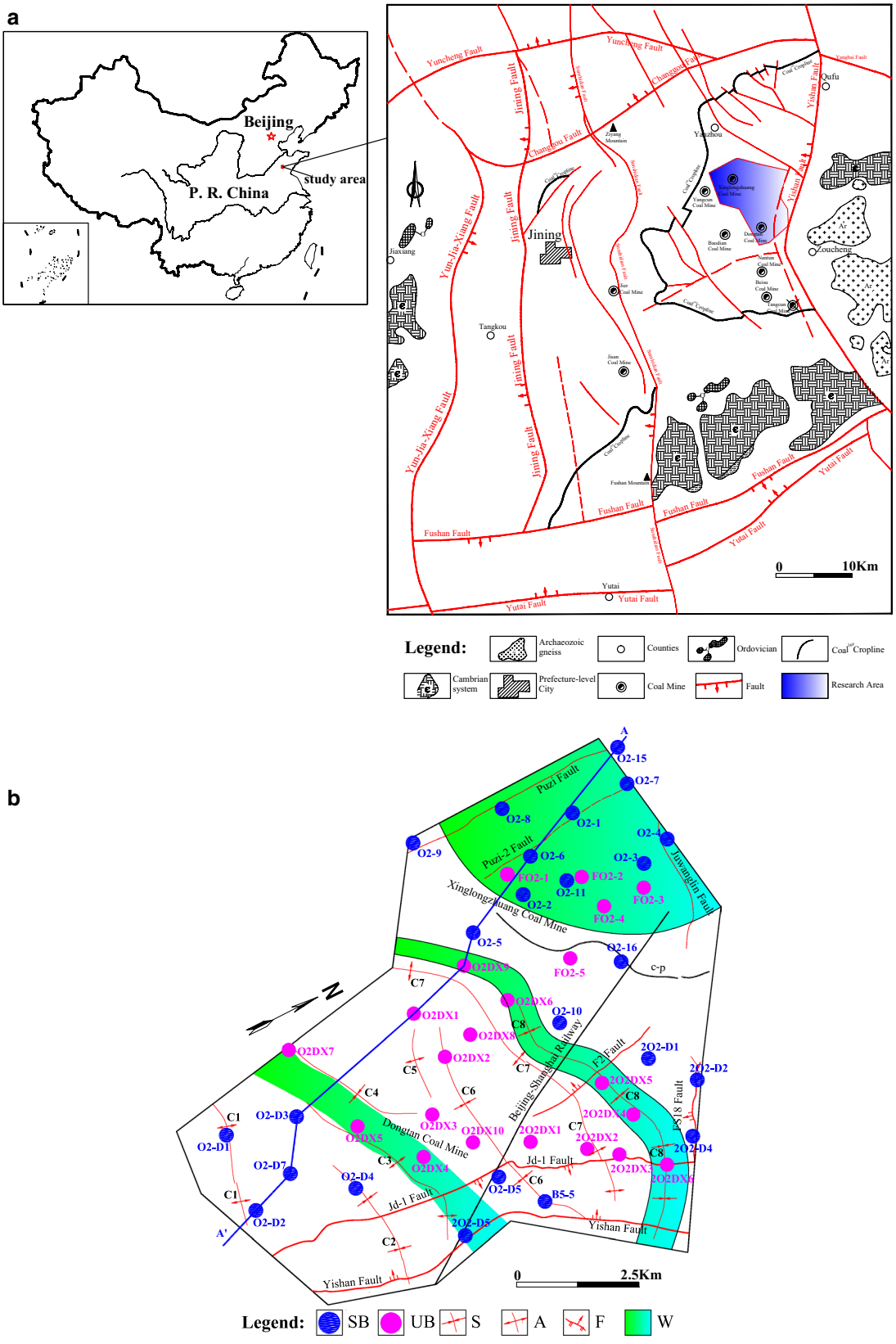

Fig. 1 **a** Hydrogeological map of the Yanzhou coal mining district, China; **b** main structures of the Xinglongzhuang-Dongtan coal mine and drilled holes in Ordovician strata. *SB* surface drilled hole, *UB* underground drilled hole, *S* syncline, *A* anticline, *F* fault, *W* water-rich area

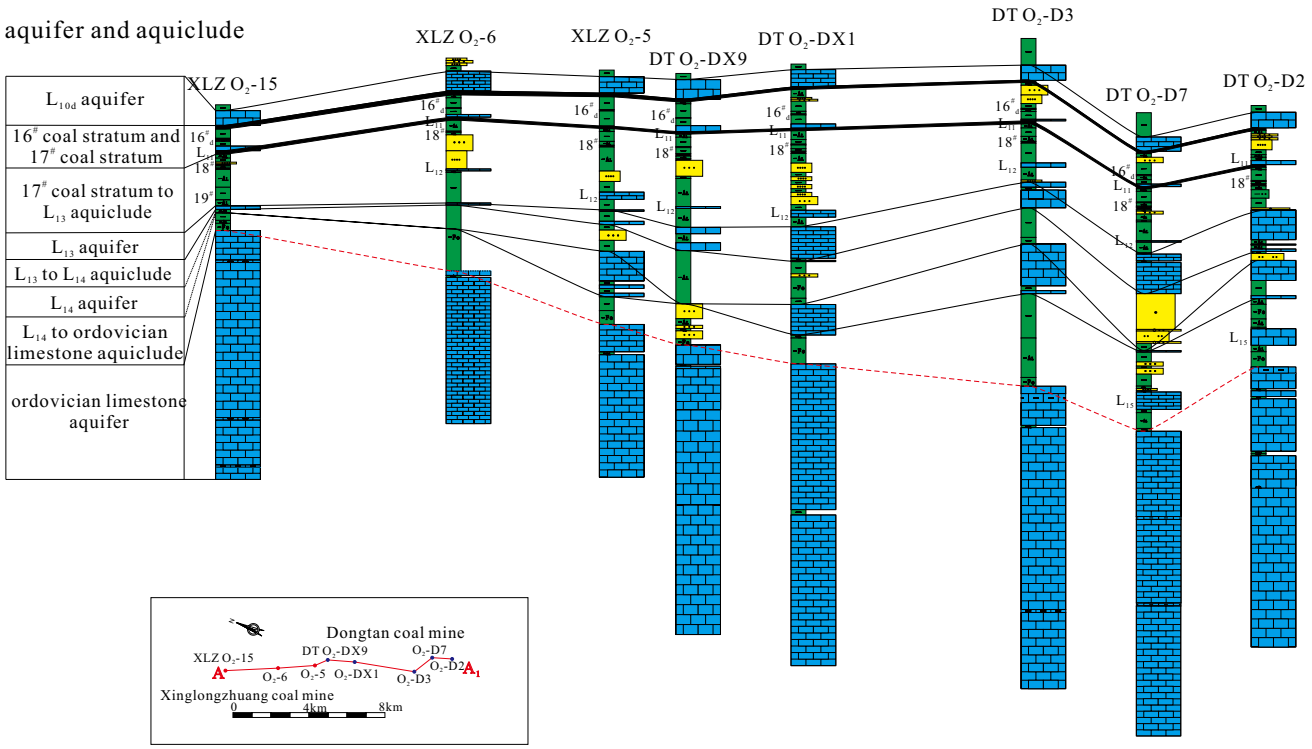

Fig. 2 Cross-section of the Xinglongzhuang–Dongtan coal mine

a complete PCA: select variables and data input; standardize the data; calculate the correlation coefficient matrix; calculate the eigenvalue of the matrix; calculate the principal component loading matrix; and, finally, calculate the parameter scoring weights (Li et al. 2013b).

Micro-porosity Test

Mercury intrusion porosimetry (MIP) testing generates capillary pressure curves, which provide large amounts of information on the void structure of porous media and micro-pore structures (Cerepi et al. 2002; Torabi et al. 2013). We used MIP (AutoPore IV 9500 V1.09 porosimeter, Micromeritics Instrument Corp., Norcross, GA, USA) to measure several pore structure characteristics of the rock samples, including porosity, total pore surface area, and median pore diameter by area and by volume. All dried rock samples were kept in desiccators before MIP analysis.

Deep karst fissures are difficult to identify from borehole cores in Ordovician limestone unless the borehole has penetrated a karst fissure zone or fault zone. The intensity of karst development in a borehole core and its surrounding space is a key factor indicating the hydrodynamics; these dynamics are reflected by the porosity of the micro-pores. Different sized pores require different mercury intrusion pressures; the larger the pore size, the lower the mercury intrusion pressure. There are four types of pores: massive, medium, tiny, and ultra-micro capillary. Massive pores, which are granular dissolved pores, are larger than 1000 μm. Medium pores, which are intergranular pores, range in size from 10 to 1000 μm. Tiny pores are inner-particle pores, and range in size from 0.1 to 10 μm. Ultra-micro capillary pores, which are intragranular pores, are less than 0.1 μm in size.

Hydrogeological Parameters

Water inflow into a drilling unit (q) reflects the recharging ability of the aquifer and is an accepted index in China for evaluating an aquifer's water yield (State Administration of Coal Mine Safety 2009). Aquifer pumping tests are a common way to obtain q; the standard pumping aperture is 91 mm and the standard drawdown is 10 m (Li and Qian 2013; Li et al. 2014a, b). An abundantly recharging water resource decreases dissolved matter concentrations, and may accelerate water–rock interactions. The index of q is $Q(10)/10$, which is based on the pumping water yield when the drawdown during drilling is 10 m. A weak water yield is $q \leq 0.1$ L (s m), a moderate water yield is 0.1 L (s m) $< q \leq 1.0$ L (s m), a strong weak water yield is 1.0 L (s m) $< q \leq 5.0$ L (s m), and a very strong water yield is $q > 5.0$ L (s m).

To obtain hydrodynamic parameters of the deep Ordovician limestone karst water in the research region, pumping tests were conducted using 24 surface and 15 underground

drilled holes. When practical pumping tests did not align with the above standards, parameters were converted into standard indices, as follows:

1. The curve for Q–S was plotted accounting for every balanced water inflow Q and drawdown S.
2. The type of empirical equation was confirmed based on the shape of the Q–S curve. The common types are linear, parabola, power function, and logarithmic function.
3. Coefficients of empirical equations were established by graphical methods or calculated.
4. The predicted water inflow $Q(10)$ was obtained based on the given drawdown of 10 m, using the empirical equation.
5. Q_{91} was calculated using Eq. (1). The standard q, which is $Q_{91}/10$, could then be established.

$$Q_{91} = Q_P\left(\frac{\lg R_P - \lg r_p}{\lg R_{91} - \lg r_{91}}\right) \quad (1)$$

where Q_{91}, R_{91}, and r_{91} are standard water inflow, radius of influence, and radius of drill hole, and Q_p, R_p, and r_p are practical water inflow, radius of influence, and radius of drill hole.

Results and Discussion

Water Chemistry

Groundwater samples were collected from 44 representative locations, and analyzed for field parameters, and major and minor ions. Cations (Ca^{2+}, Mg^{2+}, Na^{+}, and K^{+}) were analyzed using inductively coupled plasma (ICP) spectroscopy; anions (HCO_3^{-}, SO_4^{2-}, Cl^{-}) were measured using ion chromatography. Figure 3a shows that some samples fell above the equilibrium line between (Ca^{2+} + Mg^{2+}) and HCO_3^{-} (meq/L). This result indicates that pure carbonates

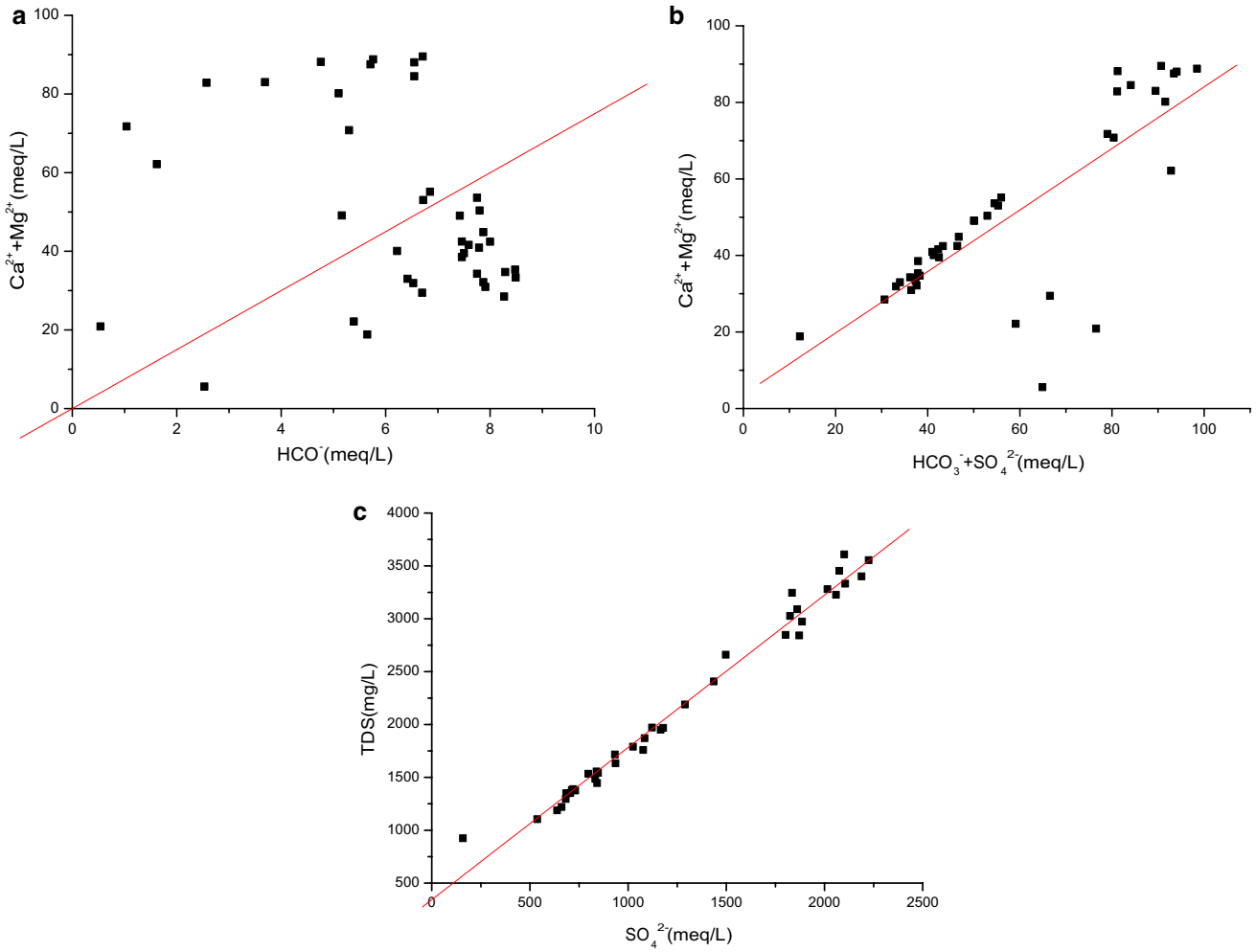

Fig. 3 **a** HCO_3^{-} vs. Ca^{2+} and Mg^{2+} (meq/L) in the karst groundwater system; **b** HCO_3^{-} and SO_4^{2-} vs. Ca^{2+} and Mg^{2+} (meq/L) in the karst groundwater system; **c** SO_4^{2-} and TDS in the karst groundwater system

are not the only source of these samples in these samples; there must be additional sources of Ca^{2+} and Mg^{2+} (Li et al. 2013a, b, 2014c, d, 2016a, b, c). As Fig. 3b shows, most of the plots of Ca^{2+} and Mg^{2+}, when compared to $HCO_3^- + SO_4^{2-}$, lie around the 1:1 trend line. This indicates that the dissolution-based weathering of sulfate rocks is an important factor in addition to carbonates (Li et al. 2016a, b, d; Wu et al. 2015).

TDS can provide important information about hydrodynamic processes and reflect regional hydrogeochemical features. Table 1 presents the TDS data, arranged from lowest to highest values by area. The degree of mineralization of the Ordovician limestone aquifer in the researched region ranges from 924.02 to 3608.74 mg/L, with variations across the area driven by environmental features.

Deep and narrow syncline structures (C8 synclines; Fig. 1b), cut by a fault in deep areas, are present. The

Table 1 Ionic concentration of Ordovician karst aquifer

Label	PH	Ca^{2+} (mg/L)	Mg^{2+} (mg/L)	Na^+ (mg/L)	K^+ (mg/L)	HCO_3^- (mg/L)	Cl^- (mg/L)	SO_4^{2-} (mg/L)	TDS (mg/L)
$2O_2$-D1	7.7	222.49	59.33	71.11	10.33	244.07	18.43	713.4	1379.03
$2O_2$-D2	7.5	232.02	60.90	48.33	7.50	263.34	17.02	693.02	1349.80
$2O_2$-D3	7.5	227.69	71.66	49.44	12.33	256.92	27.89	719.99	1388.45
$2O_2$-D4	7.4	243.80	59.40	22.00	5.33	240.27	15.45	682.56	1295.70
$2O_2$-D5	6.4	148.96	23.59	73.6	7.00	175.13	108.6	158.68	924.02
$2O_2$DX1	7.2	622.54	133.39	111.30	13.33	202.97	118.16	1861.16	3089.45
$2O_2$DX2	7.9	110.74	110.33	481.63	24.58	207.61	123.66	1436.10	2406.99
$2O_2$DX3	7.3	217.53	55.17	93.06	12.12	245.36	24.93	684.40	1349.88
2O2DX4	7.5	214.66	62.68	26.67	5.11	202.35	18.00	638.32	1187.51
$2O_2$DX5	7.8	264.63	72.35	26.09	7.67	231.23	19.38	730.95	1375.42
O_2-DX1	7.8	238.60	97.34	30.00	7.81	192.69	18.02	842.20	1445.65
O_2-DX2	9.3	117.13	54.99	760.00	25.31	16.70	211.50	1824.77	3026.88
O_2-DX3	7.3	420.81	120.49	435.00	26.25	50.10	156.97	2188.68	3400.78
O_2-DX4	7.2	568.31	157.06	152.00	17.50	114.33	148.43	2058.71	3226.73
O_2-DX5	7.2	603.02	171.01	180.00	16.25	178.56	152.70	2225.07	3554.54
O_2-DX6	7.5	290.66	80.50	43.00	6.88	231.23	20.39	935.78	1633.45
O_2-DX7	7.2	643.85	150.81	100.91	16.88	208.10	123.77	2015.18	3279.84
O_2-DX8	9.3	8.68	28.41	790.00	31.88	78.36	194.90	1497.24	2659.70
O_2-DX9	7.4	175.70	27.36	440.00	21.88	167.00	55.96	1289.29	2189.25
O_2-DX10	7.7	520.59	118.13	144.00	16.88	32.11	136.58	1871.56	2842.11
O_2-D1	7.5	509.51	119.04	135.29	15.96	164.43	92.97	1801.70	2847.03
O_2-D2	7.8	655.10	135.90	136.47	19.60	147.42	299.56	1835.03	3245.98
O_2-D3	7.4	580.81	132.56	223.08	23.37	158.00	245.65	2075.57	3453.45
O_2-D4	6.0	602.78	135.46	93.96	18.42	79.64	151.29	1885.73	2973.22
O_2-D5	7.4	611.52	158.25	118.50	17.67	176.90	128.88	2105.74	3331.11
O_2-D7	7.4	657.83	133.57	204.00	20.00	202.97	261.92	2100.52	3608.74
B5-5	7.2	230.28	73.82	35.83	8.33	262.84	20.28	705.67	1352.15
O2-1	7.7	333.36	94.36	36.92	7.88	230.15	35.88	1024.79	1789.63
O2-2	7.9	368.55	100.45	52.11	11.71	240.11	44.47	1121.52	1971.25
O2-3	7.3	304.37	86.64	58.42	11.71	243.84	49.05	932.94	1716.64
O2-4	7.7	277.45	79.11	37.84	8.42	241.35	53.62	796.97	1533.66
O2-6	7.8	371.17	108.08	44.8	9.86	212.38	42.62	1178.61	1968.22
O2-7	7.5	218.86	66.63	26.12	5.70	198.93	21.87	661.56	1220.13
O2-8	7.7	259.06	139.23	50.00	12.46	159.95	45.67	1076.92	1758.82
O2-9	7.3	340.51	97.95	41.62	9.00	241.95	38.04	1083.95	1870.27
O2-10	7.7	245.66	102.39	23.67	6.80	235.23	18.07	832.84	1486.27
O2-11	7.7	327.41	121.78	50.00	12.23	208.34	47.07	1165.56	1950.91
O2-15	7.3	193.56	54.78	21.54	5.42	256.38	20.45	537.11	1104.46
O2-16	7.8	270.66	74.66	62.96	11.92	232.54	32.33	839.12	1555.28

Ordovician limestone occurs at an elevation of − 622.3 m below the ground surface. At a depth of 203.2 m into the Ordovician limestone, the water inflow was 200 m^3/h. The water pressure in the drilled hole was 6.20 MPa, and the water pressure at the top of the limestone was 8.23 MPa. The water inflow rate exceeded 150 m^3/h in all five of the holes drilled in the Ordovician limestone in the syncline area. In contrast, water inflow was less than 5 m^3/h in the drilled holes that were 200 m away from the long and narrow syncline core.

The degree of mineralization (TDS) was less in the syncline (924.02–1388.45 mg/L) than elsewhere (1445.65–3554.54 mg/L), due to the amount of water cycling in the aquifer. The mineralization was mainly determined by SO_4^{2} mineralization, with a correlation coefficient of r = 0.99211 (Fig. 3c), was determined to be:

$$\mathrm{TDS} = 1.44\left[SO_4^{2-}\right] + 342.49 \quad (2)$$

PCA of the Data

Principal component 1 (F1) accounted for 52.43% of the total variance, and appeared to represent the water–rock interaction processes, resulting in water mineralization (Fig. 4; Table 2). Dissolution of the carbonate aquifer matrix results in high loadings of SO_4^{2-}, soluble solids, TDS, Ca, and Mg. The maximum levels of SO_4^{2-} and soluble solids point to gypsum dissolution. The principal component F2 (PC2) accounted for 15.49% of the total variance and represented high loading in pH, free carbon dioxide, and K + Na

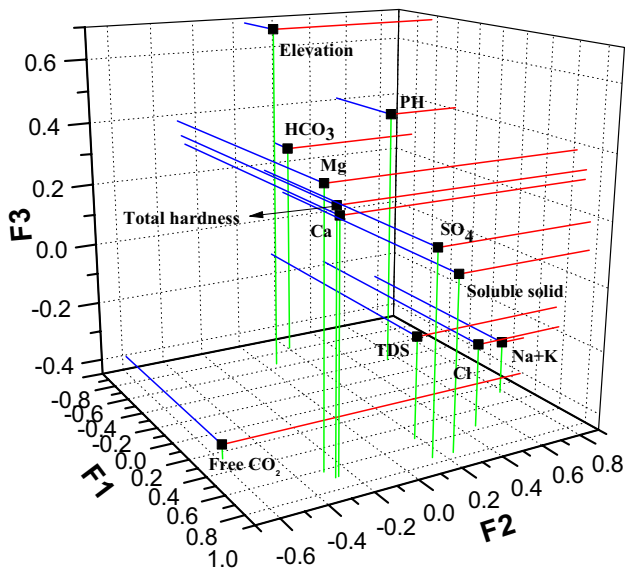

Fig. 4 Three-dimensional space diagram of principal component analysis

Table 2 Factor loadings of variables on PCs

Variable	F1	F2	F3
Elevation	− 0.457	0.059	0.685
PH	− 0.205	0.547	0.406
Total hardness	0.897	− 0.271	0.329
Free carbon dioxide	0.468	− 0.582	− 0.406
Soluble solid	0.950	0.249	0.091
TDS	0.732	0.184	− 0.128
K + Na	0.481	0.780	− 0.279
Ca	0.891	− 0.255	0.299
Mg	0.821	− 0.287	0.379
Cl	0.760	0.475	− 0.187
SO_4	0.945	0.151	0.178
HCO_3	− 0.638	0.207	0.269
Total variance (%)	52.43	15.49	11.51

(Fig. 4). PC2 highlights the importance of carbonate equilibrium in water chemistry. F3 is dominated by the influence of the sample elevations, accounting for 11.51% of the total variance. This likely reveals the dissolution of evaporate minerals and their contribution to chemical composition. The PCA analysis results indicate that deep and weak karst development is caused by limited water erosion, which is related to the deep water streamflow.

Chemical Thermodynamics Trend and Saturation Index

The water in the studied mines had pH values ranging from 6 to 9.3, representing alkaline conditions in the Ordovician strata. There were moderate Ca^{2+} and Mg^{2+} ions in the water in the mine formation, ranging from 110.74 to 657.83 mg/L (Ca^{2+}) and from 23.59 to 171.01 mg/L (Mg^{2+}), except in one well. The water had a high SO_4^{2-} concentration, ranging from 537.11 to 2225.07 mg/L, again, except in one well.

The Debye–Huckel activity model is commonly used to calculate ion activity in the water and was used in this model to calculate the Ca^{2+} and Ca^{2+}eq activity (theoretical ion of Ca^{2+}). Based on these activity data, the dissolution–precipitation tendency of carbonate minerals in the water that formed in the mine (Gibbs free energy values, ΔG) was calculated by a relevant, previously-constructed, chemical thermodynamic model (Ruan et al. 2011; Tanger and Helgeson 1988). The incremental Gibbs free energy (ΔG) for a chemical reaction is commonly used to predict the direction of a thermodynamic process and to measure the degree of reversibility. A ΔG greater than zero indicates that a process cannot occur spontaneously. A ΔG less than zero indicates a spontaneous process that cannot be reversed. The lower the ΔG value, the more easily and faster the process occurs. Based on available data on the thermodynamics of dolomite,

we calculated the ΔG of the process of dolomite dissolution under different temperatures and pressures, as a way to explain our experimental results.

Speciation modeling involves virtually calculating the chemical equilibrium of the water–rock system (Wang 1990). In this study, the speciation calculations of 20 groundwater samples were completed using the software program NETPATH. Table 3 provides the saturation indices of the minerals of concern.

The ΔG values (Fig. 5) and saturation indices (Fig. 6) of dolomite and calcite in all wells were above zero, except two (well $DT2O_2$-D5 and $XLZO_2$-D4). This means that water in

Table 3 Saturation index of water chemical composition

Label	Calcite	Dolomite	Gypsum	Label	Calcite	Dolomite	Gypsum
2O2-D1	0.71	1.19	−0.59	O2DX8	0.54	0.85	−0.73
2O2-D2	0.58	0.91	−0.59	O2DX9	0.54	0.84	−0.46
2O2-D3	0.55	0.94	−0.59	B5-5	0.27	0.39	−0.59
2O2-D4	0.46	0.65	−0.57	O2-1	0.81	1.40	−0.37
2O2-D5	−0.74	−1.94	−1.22	O2-2	1.04	1.86	−0.31
2O2DX1	0.42	0.51	−0.01	O2-3	0.41	0.62	−0.42
2O2DX5	0.56	0.89	−0.66	O2-4	0.79	1.37	−0.50
O2-D1	0.55	0.8	−0.08	O2-6	0.89	1.58	−0.30
O2-D2	0.88	1.42	−0.01	O2-7	0.44	0.71	−0.62
O2-D3	0.46	0.6	−0.02	O2-8	0.54	1.14	−0.46
O2-D4	−1.19	−2.69	−0.02	O2-9	0.44	0.67	−0.35
O2-D5	0.53	0.8	0.01	O2-10	0.72	1.40	−0.54
O2-D7	0.61	0.87	0.03	O2-11	0.73	1.38	−0.35
O2DX1	0.72	1.39	−0.54	O2-15	0.33	0.45	−0.72
O2DX2	0.5	0.73	−0.38	O2-16	0.85	1.48	−0.49
O2DX3	0.34	0.39	−0.04	FO2-1	0.25	0.32	−0.32
O2DX4	1.01	1.72	0.03	FO2-2	0.57	0.90	−0.29
O2DX5	0.53	0.73	0.02	FO2-3	0.44	0.67	−0.35
O2DX6	0.51	0.81	−0.50	FO2-4	0.35	0.50	−0.31
O2DX7	0.91	1.52	0.02	FO2-5	0.97	1.78	−0.52

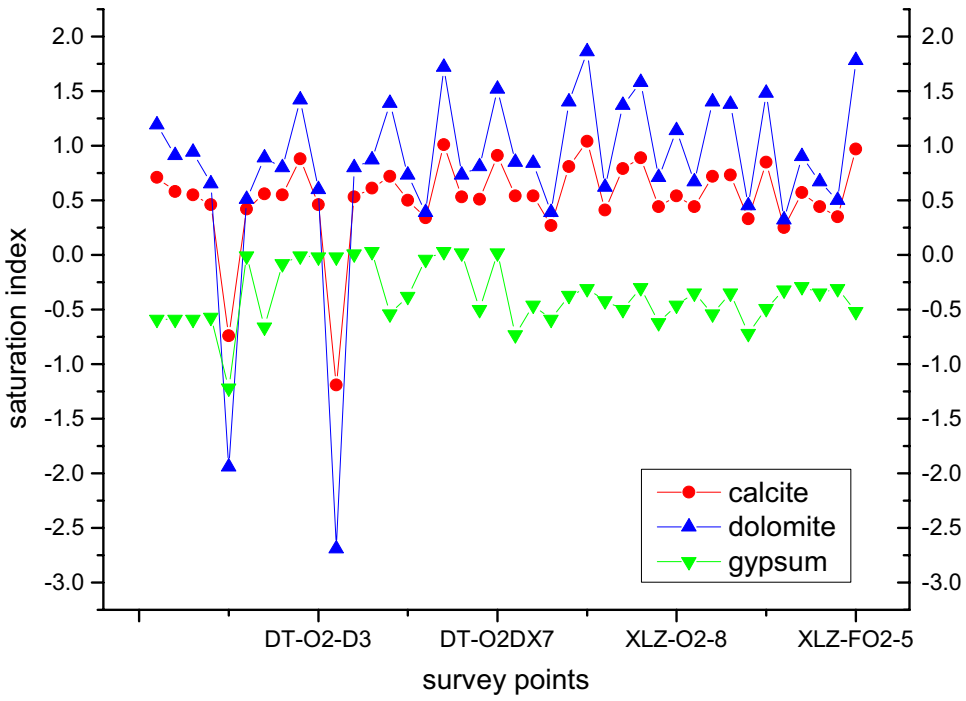

Fig. 5 Curve of saturation indices of survey points

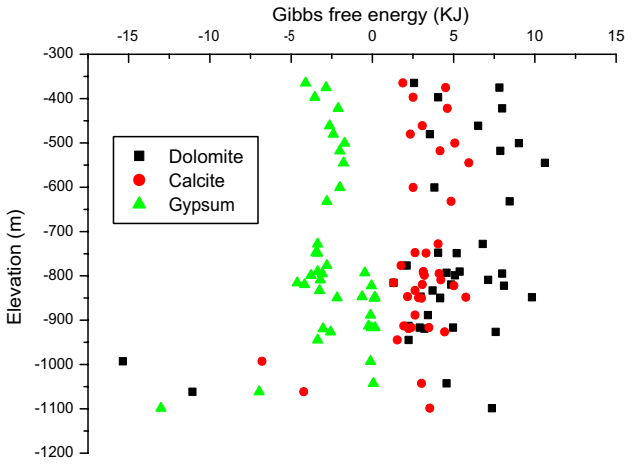

Fig. 6 Dissolution–precipitation ΔG value of dolomite, calcite, and gypsum in the Ordovician limestone

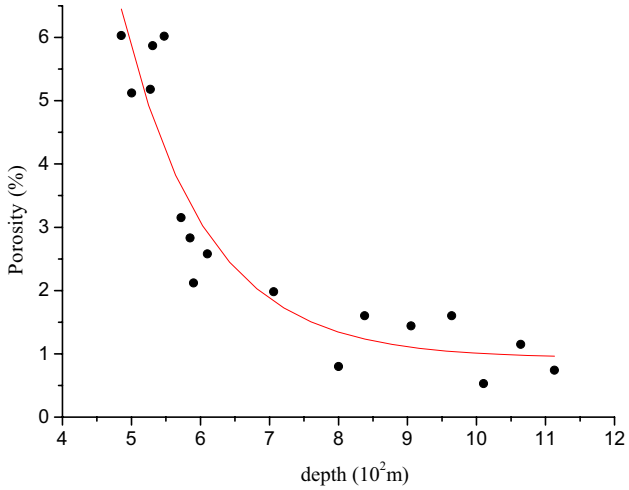

Fig. 7 Relationship between porosity and depth

the formation is suitable for dolomite and calcite precipitation. The Gibbs free energy values (ΔG) and almost all saturation indices of gypsum in all wells were below zero. This means that water in the mine formation was suited for gypsum dissolution. Thus, precipitate burial plays a role in altering the porosity and permeability of Ordovician limestone. Gypsum dissolution indicates that potential karst caves or flow zones are developing in rock rich in gypsum.

Hydrogeological Parameters and Porosity

The seepage flow decreased due to the reduced fissure opening, leading to a smaller hydraulic gradient. This made the hydrodynamic environment less beneficial for deep karst development. The porosity of the deep karst sample decreased with depth. This indicates that deep karst had formed and was retained vertically. Figure 7 shows the relationship between depth and porosity, based on the porosity of the samples at different depths. Table 4 lists the information about the 13 deep Ordovician limestone samples. Formula (3) shows the relationship between porosity n (%) and buried depth H (10^2 m).

$$n = y_0 + Ae^{-(H-x_0)/t} \quad (3)$$

where: $y_0 = 0.9306$; $A = 8.5932$; $x_0 = 4.3172$; and $t = 1.2142$.

Figure 7 shows that an increase in the buried depth affected the crack opening and porosity, which negatively impacted the development of karst structures. This, in turn, affects the amount of water in the karst fissure.

The micro-pores of the Ordovician limestone in the study area are generally medium, intergranular, and inner-particle pores. The porosity of the limestone in the Dongtan mine is less than in the Xinglongzhuang mine. The Dongtan samples for MIP testing were collected from boreholes O_2-D1, O_2-D2, and O_2-D7 in southwest Dongtan, where there is a simpler geologic structure. In contrast, the Xinglongzhuang samples came from areas with a complex geological structure. This, and the limestone aquifer depth are key factors affecting porosity.

The TDS represents the degree of mineralization in the aquifer, and indicates the aquifer's recharge and discharge intensities. The faster the water circulates, the greater the abundance of water (q), and the lower the TDS. Water circulation is the key factor affecting water abundance (q). Figure 8 shows the relationship between TDS and drilling unit water inflow (Table 5). The drilling unit water inflow values for Scope 1 are all small, i.e. $q < 0.5$ L (s m) (Fig. 8). This indicates that the abundance of water in the Ordovician aquifer within the study area is very limited, overall. The small drilling unit water inflow values for Scope 2 [0.5–1.0 L (s m)], which also have relatively low TDS values (< 2000 mg/L), are larger than for Scope 1. The drilling unit water inflow values for Scope 3 are higher yet [1.0–6.0 L (s m)]; for Scope 3, the water inflow values decrease as TDS increases.

Karst aquifer systems can generally be divided into four zones: a vertical recharge zone, a seasonal variation zone, a horizontal flow zone, and a deep, slow flow zone. The top interface of the Ordovician limestone aquifer in this area lies at 400–1000 m, in the deep slow flow zone of the karst aquifer system in a vertical flowing direction. Water inflow into the drilling unit, which represents the aquifer's water abundance, is very low. The exceptions are at the tectonically affected positions, such as the C4 and C8 syncline, C3 anticline, and the shallow area in Xinglongzhuang (Fig. 1). As such, the drilling unit water inflow generally decreases and TDS increases as the depth of the limestone increases, without the effect of geological structure. The karst cave

Table 4 Porosity of limestone

Label	Depth (m)	Quality (g)	Total amount of mercury (ml/g)	Total pore surface area (m^2/g)	Median pore diameter by volume (μm)	Median pore diameter by area (μm)	Average diameter of porosity (μm)	Porosity (%)
O2-1	485.47	5.94	0.0019	0.0013	79.99	1.07	5.61	6.03
O2-2	590.16	3.01	0.0081	0.0073	142.86	0.49	4.43	2.12
O2-2	610.25	2.77	0.0107	0.0072	212.71	0.47	5.93	2.58
O2-3	571.84	2.81	0.0119	0.0265	139.29	0.35	1.81	3.15
O2-3	585.19	2.94	0.0107	0.0053	169.44	1.11	8.09	2.83
O2-81	527.49	2.81	0.0037	0.0025	53.86	1.01	5.92	5.18
O2-8-2	547.45	3.09	0.0028	0.0009	53.88	1.55	12.26	6.02
O2-7-1	530.66	2.97	0.0044	0.0006	114.04	2.70	27.54	5.87
O2-7-2	500.21	2.87	0.0044	0.0007	107.76	9.42	23.81	5.12
O2-D1	837.95	4.34	0.0015	0.0003	41.72	6.65	17.56	1.60
O2-D2	905.39	2.98	0.0020	0.0002	86.31	22.10	43.63	1.44
O2-D7	964.22	2.04	0.0032	0.0009	17.46	7.36	15.17	1.60
B5-5	1064.00	4.49	0.0102	2.9710	13.80	9.80	13.70	1.15

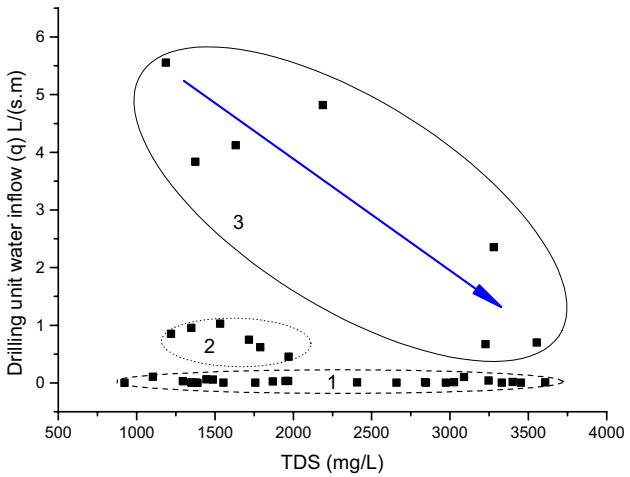

Fig. 8 Relationship between TDS and drilling unit water inflow

distribution also follows this general rule, as the number and height of karst caves vary with the elevation of the Ordovician limestone in the Zibo coal mine area, in Shandong Province, China (Fig. 9).

Conclusions

We used an integrated approach to identify and quantify the main water flow zones in a fractured karstified environment, and to describe the characteristics associated with the water chemistry and hydraulics of the Ordovician limestone aquifer. We found that the increase in the depth of buried depth impacts crack openings and porosity, and reduced crack opening and porosity negatively affect the development of

Table 5 Drilling unit water inflow

Label	Drilling unit water inflow (q) L/(s m)	Label	Drilling unit water inflow (q) L/(s m)	Label	Drilling unit water inflow (q) L/(s m)	Label	Drilling unit water inflow (q) L/(s m)
2O2-D1	0.003875	O2-D7	0.008031	O2-10	0.056000	O2-DX2	0.013000
2O2-D2	0.009298	B5-5	0.000170	O2-11	0.032000	O2-DX3	0.017000
2O2-D3	0.000945	O2-1	0.618000	O2-15	0.105000	O2-DX4	0.672000
2O2-D4	0.028112	O2-2	0.453000	O2-16	0.002300	O2-DX5	0.700000
2O2-D5	0.000042	O2-3	0.748000	2O2DX1	0.102000	O2-DX6	4.122000
O2-D1	0.001632	O2-4	1.025000	2O2DX2	0.007000	O2-DX7	2.354000
O2-D2	0.039665	O2-6	0.034000	2O2DX3	0.953000	O2-DX8	0.004000
O2-D3	0.001778	O2-7	0.852000	2O2DX4	5.556000	O2-DX9	4.819000
O2-D4	0.001884	O2-8	0.003800	2O2DX5	3.836000	O2-DX10	0.013000
O2-D5	0.003486	O2-9	0.024000	O2-DX1	0.061000		

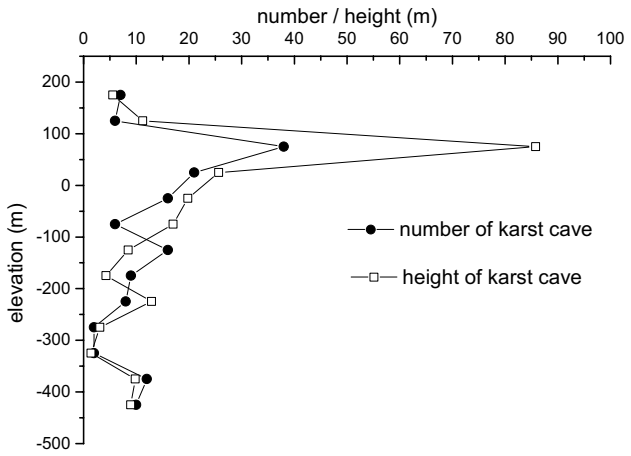

Fig. 9 Numbers and height of karst caves on different elevations

karst structures in the hydrodynamic environment. This, in turn, affects the presence of water in the karst fissure.

Water chemistry data indicated there must be additional sources of Ca^{2+} and Mg^{2+} in addition to pure carbonates. Dissolution-based weathering of sulfate rocks is an important factor. The TDS was mainly determined by the amount of SO_4^{2-}. However, in the C8 syncline zone, the TDS was 924.02–1388.45 mg/L, compared to 1445.65–3554.54 mg/L in other regions.

Therefore, mineralization in the study area demonstrates the degree of water cycling in the aquifer. Precipitate burial plays a role in the porosity and abundance of water in the Ordovician limestone. Gypsum dissolution indicates that potential karst caves or flow zones develop where there are high levels of gypsum. The PCA analysis indicates that subdued dissolution caused the deep and weak undevelopment. Fold C7–C8 in the western zone, which has abundant water, offers a high water yield ($\approx$2500 m^3/h). The integral water abundance in this area is small, except in the C8 syncline zone. The deep karst area is saturated, and the water has high SO_4^{2-} concentrations.

Acknowledgements Financial support for this work was provided by the State 973 Project (Grant 2015CB251601), the Fundamental Research Funds of the Key Program of National Natural Science of China (Grant 41430643), the Fundamental Research Funds for the Central Universities (2015QNB23), and the Priority Academic Program Development of Jiangsu Higher Education Institutions. The authors also thank the reviewers for their helpful comments.

References

Abdi H, Williams LJ (2010) Principal component analysis. Comput Stat 2(4):433–459

Bakalowicz M (2005) Karst groundwater: a challenge for new resources. Hydrogeol J 13:148–160

Bian Y-Y, Zhao D, Han Y (2017) Hydrochemical characteristics and formation mechanism of Ordovician limestone groundwater in the Yanzhou coalfield. Acta Geosci Sin 38(2):236–242

Cerepi A, Durand C, Brosse E (2002) Pore microgeometry analysis in low-resistivity sandstone reservoirs. J Petrol Sci Eng 35(3):205–232

Daher W, Pistre S, Kneppers A, Bakalowicz M, Najem W (2011) Karst and artificial recharge: theoretical and practical problems—a preliminary approach to artificial recharge assessment. J Hydrol 408(3):189–202

Davis JC (2002) Statistics and data analysis in geology, 3rd edn. Wiley Press, New York

Fidelibus MD, Tulipano L (1986) Mixing phenomena owing to sea water intrusion for the interpretation of chemical and isotopic data of discharge water in the Apulian coastal carbonate aquifer (southern Italy). In: Proceeding 9th Salt Water Intrusion Meeting, pp 591–600

Han DM, Song XF, Currell MJ, Yang JL, Xiao GQ (2014) Chemical and isotopic constraints on evolution of groundwater salinization in the coastal plain aquifer of Laizhou Bay, China. J Hydrol 508:12–27

Jiang Y (2009) Natural and anthropogenic factors affecting the groundwater quality in the Nandong karst underground river system in Yunan, China. J Contam Hydrol 109:49–61

Lang Y (2006) Geochemistry of surface and ground water in Guiyang, China: water/rock interaction and pollution in a karst hydrological system. Appl Geochem 21:887–903

Li X (2010) The use of environmental isotopic (C, Sr, S) and hydrochemical tracers to characterize anthropogenic effects on karst groundwater quality: a case study of the Shuicheng Basin, SW China. Appl Geochem 25:1924–1936

Li K (2016) Study on hydrogeologic conditions of Ordovician limestone aquifer in medium deep section of Yanzhou coal field. Coal Sci Technol 44(4):146–149

Li P, Qian H (2013) Global curve-fitting for determining the hydrogeological parameters of leaky confined aquifers by transient flow pumping test. Arab J Geosci 6(8):2745–2753

Li PY, Wu JH, Qian H (2013a) Assessment of groundwater quality for irrigation purposes and identification of hydrogeochemical evolution mechanisms in Pengyang County, China. Environ Earth Sci 69(7):2211–2225

Li PY, Qian H, Wu JH, Zhang YQ, Zhang HB (2013b) Major ion chemistry of shallow groundwater in the Dongsheng coalfield, Ordos Basin, China. Mine Water Environ 32(3):195–206

Li P, Qian H, Wu J, Liu H, Lyu X, Zhang H (2014a) Determining the optimal pumping duration of transient pumping tests for estimating hydraulic properties of leaky aquifers using global curve-fitting method: a simulation approach. Environ Earth Sci 71(1):293–299

Li P, Qian H, Wu J (2014b) Comparison of three methods of hydrogeological parameter determination in leaky aquifers using transient flow pumping tests. Hydrol Process 28(4):2293–2301

Li PY, Qian H, Wu JH, Chen J, Zhang YQ, Zhang HB (2014c) Occurrence and hydrogeochemistry of fluoride in shallow alluvial aquifer of Weihe River, China. Environ Earth Sci 71(7):3133–3145

Li P, Qian H, Wu J (2014d) Origin and assessment of groundwater pollution and associated health risk: a case study in an industrial park, northwest China. Environ Geochem Health 36(4):693–712

Li PY, Wu JH, Qian H (2016a) Hydrochemical appraisal of groundwater quality for drinking and irrigation purposes and the major influencing factors: a case study in and around Hua County, China. Arab J Geoscis 9(1):15. https://doi.org/10.1007/s12517-015-2059-1

Li PY, Wu JH, Qian H, Zhang YT, Yang N, Jing LJ, Yu PY (2016b) Hydrogeochemical characterization of groundwater in and around

a wastewater irrigated forest in the southeastern edge of the Tenger Desert, northwest China. Expos Health 8(3):331–348

Li P, Zhang Y, Yang N, Jing L, Yu P (2016c) Major ion chemistry and quality assessment of groundwater in and around a mountainous tourist town of China. Expos Health 8(2):239–252

Li PY, Li XY, Meng XY, Li MN, Zhang YT (2016d) Appraising groundwater quality and health risks from contamination in a semiarid region of northwest China. Expos Health 8(3):361–379

López-Chicano M (2001) Factors which determine the hydrogeochemical behaviour of karstic springs. a case study from the Betic Cordilleras, Spain. Appl Geochem 16:1179–1192

Niu CC, Wang Q, Wen XY, Guo Y, Zhagn PL, Zhu RY, He XH (2011) Application of principal component analysis to evaluation of black soil degradation in Jilin. Glob Geol 14(1):54–58

Qiao W, Li W, Zhang X (2014) Characteristic of water chemistry and hydrodynamics of deep karst and its influence on deep coal mining. Arab J Geosci 7:1261–1275

Reddy AGS (2013) Evaluation of hydrogeochemical characteristics of phreatic alluvial aquifers in southeastern coastal belt of Prakasam district, South India. Environ Earth Sci 68(2):471–485

Ruan Z, Yu BS, Li ZH, Zhu XM (2011) Thermodynamic equilibrium of calcite in strata environment and its application of burial karst forecasting in Tahe oil field, Tarim basin (abstract). J Jilin Univ 41(4):1020–1027

Srinivasamoorthy K, Gopinath M, Chidambaram S, Vasanthavigar M, Sarma VS (2014) Hydrochemical characterization and quality appraisal of groundwater from Pungar sub basin, Tamilnadu, India. J King Saud Univ Sci 26(1):37–52

State Administration of Coal Mine Safety (2009) Interpretation of coal mine water control regulations. China Univ of Mining and Technology Press, Beijing

Stetzenbach KJ, Hodge VF, Guo C, Farnham IM, Johannesson KH (2001) Geochemical and statistical evidence of deep carbonate groundwater within overlying volcanic rock aquifers/aquitards of southern Nevada, USA. J Hydrol 243:254–271

Tanger JC, Helgeson HC (1988) Calculation of the thermodynamic and transport properties of aqueous species at high pressures and temperatures: revised equations of state for the standard partial molal properties of ions and electrolytes. Am J Sci 288:19–98

Torabi A, Fossen H, Braathen A (2013) Insight into petrophysical properties of deformed sandstone reservoirs. AAPG Bull 97(4):619–637

Wang G (1990) Calculation of water-mineral reactions. Hydrogeol Eng Geol l: 41–45 **(in Chinese)**

Wu Q, Wang M (2006) Characterization of water bursting and discharge into underground mines with multi-layered groundwater flow systems in the north China coal basin. Hydrogeol J 14(6):882–893

Wu Q, Wang M, Wu X (2004) Investigations of groundwater bursting into coal mine seam floors from fault zones. Int J Rock Mech Min Sci 41(4):557–571

Wu Q, Fan S, Zhou W, Liu S (2013) Application of the analytic hierarchy process to assessment of water inrush: a case study for the no. 17 coal seam in the Sanhejian coal mine, China. Mine Water Environ 32:229–238

Wu J, Li P, Qian H, Duan Z, Zhang X (2014) Using correlation and multivariate statistical analysis to identify hydrogeochemical processes affecting the major ion chemistry of waters: case study in Laohebaphosphorite mine in Sichuan, China. Arab J Geosci 7(10):3973–3982

Wu J, Li P, Qian H (2015) Hydrochemical characterization of drinking groundwater with special reference to fluoride in an arid area of China and the control of aquifer leakage on its concentrations. Environ Earth Sci 73(12):8575–8588

Yu P (1994) Surface collapse in the karst mining areas in China. Mine Water Environ 13(2):21–26

Yu B, Zhu W, Xu J (2007) Numerical simulation of surface subsidence induced by deep mining. J Min Saf Eng 24(4):422–426

Zargham M (2009) Assessing hydrochemical evolution of groundwater in limestone terrain via principal component analysis. Environ Earth Sci 59:429–439